On the Relative Role of the Physical Mechanisms on Complex Biodamage Induced by Carbon Irradiation (Supporting Information)

Simone Taioli[a,b,c,*] Paolo E. Trevisanutto[a,b,d], Pablo de Vera[a,b,e], Stefano Simonucci[f,g], Isabel Abril[h], Rafael Garcia-Molina[e], and Maurizio Dapor[a,b†]

[a] *European Centre for Theoretical Studies in Nuclear Physics and Related Areas (ECT*-FBK)*
[b] *Trento Institute for Fundamental Physics and Applications (TIFPA-INFN), Trento, Italy*
[c] *Peter the Great St. Petersburg Polytechnic University, Russia*
[d] *Center for Information Technology, Bruno Kessler Foundation, Trento, Italy*
[e] *Departamento de Física, Centro de Investigación en Óptica y Nanofísica, Universidad de Murcia, Spain*
[f] *School of Science and Technology, University of Camerino, Italy*
[g] *INFN, Sezione di Perugia, Italy and*
[h] *Departament de Física Aplicada, Universitat d'Alacant, Spain*

* taioli@ectstar.eu
† dapor@ectstar.eu

TDDFT calculation of the ELF of liquid water

The energy loss function (ELF) of a material provides its electronic excitation spectrum in the momentum and energy space $(\hbar k, E)$. It is obtained from its complex dielectric function $\epsilon(k, E)$ as $\mathrm{Im}[-1/\epsilon(k, E)]$.

Liquid water is the epitome of amorphous systems showing a large degree of randomness. To cut-off the prohibitively expensive computational task of realizing an ensemble of statistically-independent optimized water configurations, we assumed that a single snapshot of the liquid water configuration is enough to obtain its energy loss function $\mathrm{ELF}(\hbar k, E)$, which gives access to its electronic excitation spectrum as a function of momentum and energy $(\hbar k, E)$. This relies on previous photoabsorption spectra simulations of liquid water, where different molecular arrangements showed similar optical response [1].

A water supercell was generated by carrying out molecular dynamics (MD) simulations with several thousands molecules, using the empirical TIP3P force-field [2] implemented in the LAMMPS package [3]. The simulations ran for 100 ps, the first 10 ps being due to reach thermodynamic equilibrium at the temperature of 300 K. A cubic cell with side of 0.985 nm that can accommodate 32 water molecules to reproduce the experimental water density at room conditions ($\rho = 1$ g/cm^3) was then obtained. The latter cell size is a trade-off between reasonable computational effort of the many-body calculations and good agreement with experimental ELF data [4–6]. Finally, this super cell was further relaxed imposing periodic boundary conditions below 10^{-3} Ry/Å for the interatomic forces via first-principles density functional theory (DFT) calculations [7] as implemented in the Quantum Espresso code suite [8], using a PBE-GGA functional [9] for both O and H. We have used the Troullier-Martins (TM) norm-conserving pseudopotentials tabulated in the Quantum Espresso web page. With the Monkhorst-Pack mesh grid with only comprised of the Γ point and the (kinetic) energy cut-off of 130 Ry, the self consistent DFT convergence is reached within the energy error of 10^{-5}. The optimized water configuration used in this work appears in Fig. S1.

First principles simulations of the ELF of liquid water were carried out in the energy range $0 \leq E \leq 100$ eV for momentum transfers $0 \leq \hbar k \leq 2.5$ a.u., with a resolution of 0.25 a.u. Due to the random orientation of water molecules, only the dependence on the wave vector module k was considered in the ab-initio calculations, performed by the Linear Response (LR)-TDDFT approach [10]. In the linear response approximation the susceptibility $\chi(k, E)$ of the medium is determined via the relation:

$$\chi^{-1}(k, E) = \chi_0^{-1}(k, E) - v_{\mathrm{C}}(k) - f_{\mathrm{xc}}(k, E)\,, \tag{S1}$$

where $\chi_0^{-1}(k, E)$ is the non-interacting susceptibility, $v_{\mathrm{C}}(k)$ is the bare Coulomb interaction and $f_{\mathrm{xc}}(k, E)$ is the TD-DFT kernel. In our calculations, we have employed the Adiabatic PBE (APBE) kernel [11] to include the electron-hole and electron-electron interactions in the ELF spectra. The dielectric matrix $\epsilon(k, E)$ is related to the $\chi(k, E)$ by:

$$\epsilon(k, E) = 1 - v_{\mathrm{C}}(k)\chi(k, E)\,. \tag{S2}$$

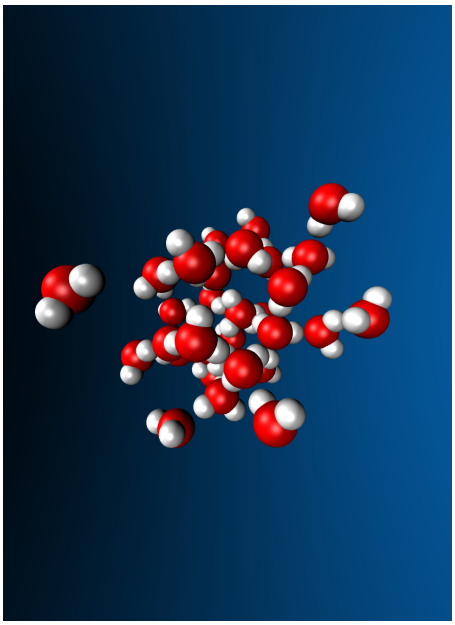

FIG. S1. Optimized water configuration used to calculate the ELF via TDDFT.

The ELF spectra are determined with the Lanczos chains algorithm (LCA), implemented in the turboEELS code [12]. LCA main advantage is that allows to avoid the sum over the excited states. The water ELF converged with a $4 \times 4 \times 4$ Monkhorst-Pack mesh grid and 600 Lanczos iterations.

Cross sections of inelastic and elastic events

The dielectric formalism [13–15] provides a theoretical framework to study the inelastic interactions of charged particles with matter, in such a way that the features of the projectile (charge, mass and energy) and the medium (electronic excitation spectrum, through its ELF) appear decoupled in all the expressions used. The basic quantity to study the generation and subsequent transport of electrons in a medium resulting from the interaction with a swift charged particle is the probability of transferring an energy E and a momentum $\hbar k$ to the medium, which is provided by the doubly differential cross section DDCS [13–15]:

$$\frac{\mathrm{d}^2\sigma}{\mathrm{d}E\,\mathrm{d}k} = \frac{e^2}{\pi\hbar\mathcal{N}}\frac{M[Z-\rho_Q(k)]^2}{T}\frac{1}{k}\,\mathrm{ELF}(k,E)\,, \tag{S3}$$

where Z, M, and T are the atomic number, mass and energy for the case of an incident ion; the charge state Q of the ion is accounted for through the Fourier transform $\rho_Q(k)$ of its electronic density. The response of the medium to the perturbation created by the external charged particles is provided by its energy loss function $\mathrm{ELF}(k,E)$.

The number of generated electrons, their energy and angular distributions can be obtained from the DDCS (S3) for a carbon ion by integration through energy and/or momentum transfer, or a suitable transformation to obtain the dependence in ejection angle [16, 17]. The energy E delivered by the charged projectile to the electronic degrees of freedom of the medium is related to the energy W of an ejected electron through $E = B + W$, with B being the mean binding energy of the outer-shell electrons, which discriminates whether an excitation (if $E < B$) or an ionization (if $E > B$) occurs [16–18]. Expression (S3) can be also used to determine the cross sections for ionization and excitation due to electron impact by replacing the ion characteristics by the electron ones ($M = m$, $Z - \rho_Q(k) = 1$) and, additionally, by suitably choosing the integration limits and accounting for exchange and indistinguishability effects [18].

The elastic cross sections for an electron moving through a medium can be obtained via two different approaches: the Mott theory [19], by using a best fit of data from Hartree-Fock simulations in a central field, or by direct solution of the Dirac equation in a multi-centric functional space [20–22] to account for the randomly oriented molecular system.

Using the former approach, the differential elastic scattering cross-section of electrons impinging on randomly oriented molecules can be written [23]:

$$\frac{d\sigma_{\mathrm{el}}}{d\Omega} = \sum_{m,n}\frac{\sin(kr_{mn})}{kr_{mn}}[f_m(\theta)f_n^*(\theta) + g_m(\theta)g_n^*(\theta)]\,, \tag{S4}$$

where $f_{m,n}, g_{m,n}$ are the direct and spin-flip scattering amplitudes of species m, n; k and θ are the momentum transfer and scattering angle, respectively. In the specific case of randomly oriented liquid water molecules, Eq. (S4) reads:

$$\begin{aligned}\left(\frac{d\sigma_{\mathrm{el}}}{d\Omega}\right)_{\mathrm{H_2O}} &= 2\left(\frac{d\sigma_{\mathrm{el}}}{d\Omega}\right)_{\mathrm{H}} + \left(\frac{d\sigma_{\mathrm{el}}}{d\Omega}\right)_{\mathrm{O}} + \\ &+ 2\,\frac{\sin kr_{\mathrm{OH}}}{kr_{\mathrm{OH}}}[f_{\mathrm{H}}(\theta)f_{\mathrm{O}}^*(\theta) + f_{\mathrm{O}}(\theta)f_{\mathrm{H}}^*(\theta) + g_{\mathrm{H}}(\theta)g_{\mathrm{O}}^*(\theta) + g_{\mathrm{O}}(\theta)g_{\mathrm{H}}^*(\theta)] + \\ &+ 2\frac{\sin kr_{\mathrm{HH}}}{kr_{\mathrm{HH}}}[|f_{\mathrm{H}}(\theta)|^2 + |g_{\mathrm{H}}(\theta)|^2]\,,\end{aligned} \tag{S5}$$

where $r_{\mathrm{OH}} = 0.9584$ Å and $r_{\mathrm{HH}} = 1.5151$ Å are the equilibrium bond lengths of water molecule, $f_{\mathrm{O,H}}(\theta)$, $g_{\mathrm{O,H}}(\theta)$ are the direct and spin-flip scattering amplitudes of O and H. The first and second terms describe the atomic independent contribution to the differential elastic cross-section, while the third and fourth terms include the interference between elastically scattered electron waves emerging from the atomic constituents of water.

The first-principles approach to the elastic cross section calculation is based on the self-consistent solution of the Dirac equation using the Hartree-Fock approximation within a functional space spanned by a Gaussian basis set. The Dirac-Hartree-Fock (DHF) equation of many particles systems can be written [24]:

$$\begin{pmatrix} mc^2 + V - E & -c\boldsymbol{\sigma}\cdot i\boldsymbol{\nabla} \\ -c\boldsymbol{\sigma}\cdot i\boldsymbol{\nabla} & -mc^2 + V - E \end{pmatrix}\begin{pmatrix}\psi_{\mathrm{L}} \\ \psi_{\mathrm{S}}\end{pmatrix} = 0\,, \tag{S6}$$

where m is the electron mass, $\boldsymbol{\sigma}$ are the Pauli matrices, V is the Coulomb potential, and $\psi_{\mathrm{L,S}}$ are the large and small components of the quadrivector, respectively. The DHF Hamiltonian can be projected into a functional space by means of Gaussian functions [22, 24, 25], which are identified by an exponent α and centered in $\mathbf{R}$:

$$g\left(\alpha,\mathbf{R};\mathbf{r}\right)=\left(\frac{2\alpha}{\pi}\right)^{\frac{3}{4}}e^{-\alpha(\mathbf{r}-\mathbf{R})^{2}}\,. \tag{S7}$$

Using Gaussian functions one can analytically calculate [24] mono-electronic:

$$\int d\mathbf{r}\frac{1}{r}g\left(\alpha,\mathbf{R};\mathbf{r}\right)=\left(\frac{\pi}{\alpha}\right)^{\frac{3}{2}}\frac{\mathrm{erf}\left(\sqrt{\alpha}R\right)}{R}=\left\langle g\frac{1}{r}\right\rangle\,, \tag{S8}$$

and bi-electronic integrals for the Coulomb potential:

$$\begin{aligned}\left\langle s_1s_3\left|\frac{e^{-\frac{\left|\mathbf{r}-\mathbf{r}'\right|}{\xi}}}{\left|\mathbf{r}-\mathbf{r}'\right|}\right|s_2s_4\right\rangle&=\left(\frac{2\alpha_1}{\pi}\right)^{\frac{3}{4}}\left(\frac{2\alpha_2}{\pi}\right)^{\frac{3}{4}}\left(\frac{2\alpha_3}{\pi}\right)^{\frac{3}{4}}\left(\frac{2\alpha_4}{\pi}\right)^{\frac{3}{4}}\\&\cdot\int d\mathbf{r}\int d\mathbf{r}'e^{-\alpha_1(\mathbf{r}-\mathbf{R}_1)^2}e^{-\alpha_2(\mathbf{r}-\mathbf{R}_2)^2}e^{-\alpha_3\left(\mathbf{r}'-\mathbf{R}_3\right)^2}e^{-\alpha_4\left(\mathbf{r}'-\mathbf{R}_4\right)^2}\\&=\left[\frac{2\left(\alpha_1\alpha_2\alpha_3\alpha_4\right)^{\frac{1}{4}}}{\pi}\right]^3e^{-\frac{\alpha_1\alpha_2}{\alpha_1+\alpha_2}(\mathbf{R}_1-\mathbf{R}_2)}e^{-\frac{\alpha_3\alpha_4}{\alpha_3+\alpha_4}(\mathbf{R}_3-\mathbf{R}_4)}\\&\cdot\int d\mathbf{r}\int d\mathbf{r}'e^{-(\alpha_1+\alpha_2)(\mathbf{r}-\mathbf{P}_{12})^2}e^{-(\alpha_3+\alpha_4)\left(\mathbf{r}'-\mathbf{P}_{34}\right)^2}\frac{e^{-\frac{\left|\mathbf{r}-\mathbf{r}'\right|}{\xi}}}{\left|\mathbf{r}-\mathbf{r}'\right|}\,,\end{aligned} \tag{S9}$$

where $\mathbf{P}_{12}=\frac{\alpha_1\mathbf{R}_1+\alpha_2\mathbf{R}_2}{\alpha_1+\alpha_2}$, $\mathbf{P}_{34}=\frac{\alpha_3\mathbf{R}_3+\alpha_4\mathbf{R}_4}{\alpha_3+\alpha_4}$, α_i $(i=1,2,3,4)$ are the Dirac matrices. By defining $\mathbf{s}=\frac{\mathbf{r}+\mathbf{r}'}{2}$ and $\mathbf{q}=\mathbf{r}-\mathbf{r}'$ we obtain:

$$\begin{aligned}&\int d\mathbf{r}\int d\mathbf{r}'e^{-(\alpha_1+\alpha_2)(\mathbf{r}-\mathbf{P}_{12})^2}e^{-(\alpha_3+\alpha_4)\left(\mathbf{r}'-\mathbf{P}_{34}\right)^2}\frac{e^{-\frac{\left|\mathbf{r}-\mathbf{r}'\right|}{\xi}}}{\left|\mathbf{r}-\mathbf{r}'\right|}\\&\qquad=\int d\mathbf{s}\int d\mathbf{q}e^{-(\alpha_1+\alpha_2)\left(\mathbf{s}+\frac{\mathbf{q}}{2}-\mathbf{P}_{12}\right)^2}e^{-(\alpha_3+\alpha_4)\left(\mathbf{s}-\frac{\mathbf{q}}{2}-\mathbf{P}_{34}\right)^2}\frac{e^{-\frac{q}{\xi}}}{q}\\&\qquad=\left(\frac{\pi}{\alpha_1+\alpha_2+\alpha_3+\alpha_4}\right)^{\frac{3}{2}}\int d\mathbf{q}e^{-\frac{(\alpha_1+\alpha_2)(\alpha_3+\alpha_4)}{\alpha_1+\alpha_2+\alpha_3+\alpha_4}\left[\mathbf{q}-(\mathbf{P}_{12}-\mathbf{P}_{34})\right]^2}\frac{e^{-\frac{q}{\xi}}}{q}\,.\end{aligned}$$

Mono- and bi-electronic integrals, for dealing with the electron-electron interaction, can be also modeled by a Yukawa potential with an exponential coefficient equal to zero [24]. A self-consistent solution of the DHF equations leads to the knowledge of the Hamiltonian spectrum. To account for multiple scattering from surrounding water molecules in liquid phase we used our projected potential approach [22, 25] on a cluster of six water molecules, which keeps reasonable the computational cost. In particular, wavefunctions and self-consistent potentials are expanded in a basis set of aug-cc-pVTZ Gaussian functions (GBS), centered into the nuclei. Mono– and bi– electronic molecular integrals are computed at each self-consistent cycle among the GBS functions, and then through a unitary transformation in the molecular orbital basis [24]. Only the potential term in the Dirac Hamiltonian is projected onto the finite set of L^2 functions to recover the continuum. The multi-scattering interference terms are inherently included in the formalism. The differential elastic cross section for solid angle unit is then obtained as follows:

$$\frac{\mathrm{d}\sigma}{\mathrm{d}\Omega}=\frac{m^2}{4\pi^2}|\langle\phi_{k\hat{n}}|T^+(E)|\phi_{\mathbf{k}}\rangle|^2=\frac{m^2}{4\pi^2}|\langle\phi_{k\hat{n}}|V|\psi^+_{\mathbf{k}}(\mathbf{r}')\rangle|^2\,, \tag{S10}$$

where $\phi_{k\hat{n}}$ is the asymptotic incoming plane-wave impinging on the water cluster with momentum k in the direction $\hat{n}$, $\phi_{\mathbf{k}}$ is the asymptotic outgoing free plane wave in the scattering direction $\mathbf{k}$, $T^+(E)$ is the on-shell T-matrix, V is the self-consistent molecular potential obtained by the solution of the DHF equations, and $\psi^+_{\mathbf{k}}(\mathbf{r}')=\exp(\mathrm{i}\mathbf{kr})-\frac{m}{2\pi}\frac{\exp(\mathrm{i}\mathbf{kr})}{r}\psi^+_{\mathbf{k}}(\mathbf{r}')$ is the scattering wavefunction. Since V is the approximate representation of the long range Coulomb potential projected on a finite functional space, one can replace $\psi^+_{\mathbf{k}}$ with $\phi_{\mathbf{k}}$ outside the scattering volume where the potential dies off (Born approximation) [22, 25].

Generation, transport and effects of secondary electrons

Monte Carlo simulations at each carbon kinetic energy T were carried out using 1200 ion tracks of 50 nm length each one, with different random seeds at each ion shot. The latter path length was chosen so that virtually all the secondary electrons generated along the carbon ion track can reach the sensitive volume (having dimensions of a DNA-like target), while keeping simulation times within reasonable limits. To achieve an acceptable trade-off between computational cost and low signal-to-noise ratio, we assume that 1000 electrons are generated initially along the track at each collision between the carbon ion and the water target. In average, carbon ions undergo 30 (1 GeV) to 1000 (0.2 MeV/u) collisions; thus each ion shot produces on average 10^5–10^6 electrons. These electrons then scatter within the target material, producing an average number of 100 further electrons each, before stopping; multiplying by the number of ion shots (1200) our simulations are equivalent to assess 4 to 100 billion electron trajectories, which were followed up by means of the Monte Carlo code SEED (Secondary Electron Energy Deposition) [26, 27] until absorption in the medium. Deviation of the electron trajectory was accounted for through the elastic cross section, and different inelastic events (ionization, excitation, DEA, electron-phonon and electron-polaron) were drawn according to their relative probability $p_i = (\sum_i \Lambda_i)/\Lambda_i$, where Λ_i is the inverse mean free path between two collisional events of the i type, using a Bortz, Kalos and Lebowitz (BKL) acceptance algorithm [28, 29]. At low energy, a significant contribution to the total inelastic scattering cross section is given by the electron-polaron and the electron-phonon interactions. These energy losses are dealt with phenomenologically by introducing, respectively, mean free paths (i) for polaron trapping $\lambda_{\rm trap}^{-1} = C_{\rm trap}\exp(-\gamma_{\rm trap}W)$, where $C_{\rm trap} = 0.1$ nm^{-1} and $\gamma_{\rm trap} = 0.1$ eV^{-1}; (ii) and for electron-phonon couplings as described by the Fröhlich theory [30, 31].

The probability of having a scattering process i, be it elastic or inelastic, is compared with a random number and the type of collision is selected. Depending on the event, the electron trajectory and energy are modified. To determine the nanodosimetric observables presented in this work, the possible damaging events (ionization, excitation or DEA) are scored only when occurring inside the sensitive volume for each distance from the ion track.

REFERENCES

[1] V. Garbuio, M. Cascella, L. Reining, R. D. Sole, and O. Pulci, Physical Review Letters **97**, 137402 (2006).
[2] A. D. MacKerell, D. Bashford, M. Bellott, R. L. Dunbrack, J. D. Evanseck, M. J. Field, S. Fischer, J. Gao, H. Guo, S. Ha, D. Joseph-McCarthy, L. Kuchnir, K. Kuczera, F. T. K. Lau, C. Mattos, S. Michnick, T. Ngo, D. T. Nguyen, B. Prodhom, W. E. Reiher, B. Roux, M. Schlenkrich, J. C. Smith, R. Stote, J. Straub, M. Watanabe, J. Wiórkiewicz-Kuczera, D. Yin, and M. Karplus, Journal of Physical Chemistry B **102**, 3586 (1998).
[3] M. Senn, *LAMMPS Molecular Dynamics Simulator*, Sandia National Laboratories (2020).
[4] N. Watanabe, H. Hayashi, and Y. Udagawa, Bulletin of the Chemical Society of Japan **70**, 719 (1997).
[5] H. Hayashi, N. Watanabe, Y. Udagawa, and C. Kao, Proceedings of the National Academy of Sciences of the United States of America **97**, 6264 (2000).
[6] N. Watanabe, H. Hayashi, and Y. Udagawa, Journal of Physics and Chemistry of Solids **61**, 407–409 (2000).
[7] P. Hohenberg and W. Kohn, Physical Review **136**, B864 (1964).
[8] P. Giannozzi and et al., Journal of Physics: Condensed Matter **21**, 395502 (2009).
[9] J. P. Perdew, K. Burke, and M. Ernzerhof, Physical Review Letters **77**, 3865 (1996).
[10] G. Onida, L. Reining, and A. Rubio, Reviews of Modern Physics **74**, 601 (2002).
[11] T. Olsen, C. E. Patrick, J. E. Bates, A. Ruzsinszky, and K. S. Thygesen, npj Computational Materials **5**, 106 (2019).
[12] I. Timrov, N. Vast, R. Gebauer, and S. Baroni, Computer Physics Communications **196**, 460 (2015).
[13] J. Lindhard, Det Kongelige Danske Videnskabernes Selskab Matematisk-fysiske Meddelelser **28(8)**, 1 (1954).
[14] R. H. Ritchie, Physical Review **114**, 644 (1959).
[15] H. Nikjoo, S. Uehara, and D. Emfietzoglou, *Interaction of radiation with matter* (CRC Press, Boca Raton, FL, 2012).
[16] P. de Vera, R. Garcia-Molina, I. Abril, and A. V. Solov'yov, Physical Review Letters **110**, 148104 (2013).
[17] P. de Vera, R. Garcia-Molina, and I. Abril, Physical Review Letters **114**, 018101 (2015).
[18] P. de Vera and R. Garcia-Molina, Journal of Physical Chemistry C **123**, 2075 (2019).
[19] N. Mott and H. Massey, *The theory of atomic collisions* (1949).
[20] S. Taioli, S. Simonucci, L. Calliari, M. Filippi, and M. Dapor, Physical Review B **79**, 085432 (2009).
[21] S. Taioli, S. Simonucci, L. Calliari, and M. Dapor, Physics reports **493**, 237 (2010).
[22] S. Taioli, S. Simonucci, and M. Dapor, Computational Science & Discovery **2**, 015002 (2009).
[23] F. Salvat, A. Jablonski, and C. J. Powell, Computer Physics Communications **165**, 157 (2005).
[24] T. Morresi, S. Taioli, and S. Simonucci, Advanced Theory and Simulations **1**, 1870030 (2018).
[25] S. Taioli, S. Simonucci, L. Calliari, and M. Dapor, Physics Reports **493**, 237 (2010).
[26] M. Dapor, I. Abril, P. de Vera, and R. Garcia-Molina, Physical Review B **96**, 064113 (2017).
[27] M. Dapor, *Transport of Energetic Electrons in Solids. Computer Simulation with Applications to Materials Analysis and Characterization, 3rd ed.* (Springer Nature Switzerland AG, 2020).
[28] S. Taioli, Journal of Molecular Modeling **20**, 2260 (2014).

[29] A. Bortz, M. Kalos, and J. Lebowitz, Journal of Computational Physics **17**, 10 (1975).
[30] H. Fröhlich, Advances in Physics **3**, 325 (1954).
[31] J. Llacer and E. L. Garwin, Journal of Applied Physics **40**, 2766 (1969).